Positional Isomers of Isocyanoazulenes as Axial Ligands Coordinated to Ruthenium(II) Tetraphenylporphyrin: Fine Tuning of Redox and Optical Properties

Mahtab Fathi-Rasekh,[a,†] Gregory T. Rohde,[b] Mason D. Hart,[c] Toshinori Nakakita,[c] Rashid Valiev,[d] Mikhail V. Barybin,*[c] and Victor N. Nemykin*[a,e]

[a] *Department of Chemistry and Biochemistry, University of Minnesota Duluth, 1039 University Drive, Duluth, MN 55812, USA,*

[b] *Marshall School, Duluth, MN, 55811 USA*

[c] *Department of Chemistry, University of Kansas, 1251 Wescoe Hall Drive, Lawrence, Kansas, 66045, USA*

[d] *Rashid's address*

[e] *Department of Chemistry, University of Manitoba, 144 Dysart Road, Winnipeg, MB, R3T 2N2, Canada*

[†] *Current address: University of California – Irvine, 1102 Natural Sciences 2, Irvine, CA 92617, USA*

ABSTRACT

Two isomeric ruthenium(II) 5,10,15,20-tetraphenylporphyrins axially coordinated to the redox-active, low-optical gap-containing 2- or 6-isocyanoazulene ligands have been prepared and characterized by NMR, UV-vis, and MCD spectroscopy methods, high-resolution mass spectrometry, and X-ray crystallography. The UV-vis and MCD spectra are suggestive of the presence of the low-energy, azulene-centered transitions in the *Q*-band region of the porphyrin chromophore. The first coordination sphere in new L_2RuTPP complexes is reflective of compressed tetragonal geometry. The redox properties of the new compounds were studied by electrochemical and spectroelectrochemical methods and correlated with the electronic structures predicted by the Density Functional Theory calculations. The experimental and theoretical data are suggestive of the low-potential reduction processes centred at the axial azulene ligands and oxidation processes centred at the ruthenium ion or porphyrin core.

INTRODUCTION

Organic isocyanides, C≡N-R, are important constituents in the coordination chemistry's ligand toolbox, particularly, because of their tuneable steric characteristics and σ-donor/π–acceptor ratio[1]. While the coordination of organic isocyanides to a variety of metalloporphyrins[2] and metallophthalocyanines[3] has been well documented, combining redox non-innocent organic and organometallic isocyanides with such transition metal platforms offers additional opportunities in the design of molecular wires.[4] Indeed, axial coordination of isocyanoferrocene and 1,1'-diisocyanoferrocene[5] to Ru(II)porphyrins and phthalocyanines has been recently shown to exert unusual redox profiles of the corresponding adducts that are attractive in the context of applications in molecular electronics[6], including molecular wires.[7,9] Isocyanoazulenes[8] constitute a special

class of isocyanoarenes and feature the non-benzenoid aromatic substituent comprised of fused 5- and 7-membered sp^2-carbon rings. The polar nature of the azulenic scaffold (*ca.* 1.0 Debye) and the position of its attachment to the isocyanide junction allows manipulating the electronic structure of transition metal - isocyanide complexes.[8] In order to expand the potential utility of isocyanoazulenes in assembling organometallic molecular wires, J. Am. Chem. Soc. 2010, 132, 15924–15926; Chem. Sci., 2016, 7, 1422-1429 in this paper, we consider two isomeric systems involving either 2-isocyanoazulene (2-CNAZ) or 6-isocyanoazulene (6-CNAz) ligands axially coordinated to the ruthenium(II) tetraphenylporphyrin (TPP) core (Scheme 1). The choice of this isomeric pair stemmed, in part, by the opposite orientation of the azulenic dipole in the isocyanoazulene ligands. The physicochemical characteristics of the new complexes L_2RuTPP (L = 2- or 6-isocyanoazulene) are compared to the "reference" compound (*t*-BuNC)$_2$RuTPP.[10]

Experimental Section

Materials

All commercial reagents were ACS grade and were used without further purification. All reactions were performed under a dry argon atmosphere within flame-dried glassware. Toluene was distilled over sodium metal. Dichloromethane (DCM) and hexanes were distilled over CaH_2. Tetrabutylammonium tetrakis(pentafluorophenyl)borate (TBAF, $(NBu_4)[B(C_6F_5)_4]$),[11] 2-isocyanoazulene (2-CNAz),[8] 6-isocyanoazulene (6-CNAz),[8] and (*t*-BuNC)$_2$RuTPP (**3**)[10] were prepared according to the literature procedures.

Synthetic work

Synthesis of (2-CNAz)$_2$RuTPP. Commercially available (OC)RuTPP (0.16 g, 0.21 mmol) was added to a solution of the 2-CNAz ligand (0.20 g, 1.3 mmol) in 20 mL of the toluene: DCM (1/1,

v/v) mixture under argon atmosphere. The reaction mixture was stirred for 2 h at room temperature. The solvent was then removed under reduced pressure. The resulting solid was washed several times with hexanes, water, and dried under vacuum. Yield: 0.13 g (59%). Elemental analysis: calculated for $C_{66}H_{42}N_6Ru \cdot H_2O$: C, 76.36; H, 4.27; N, 8.09. Found: C, 76.01; H, 4.22; N, 7.90. ^{1}H NMR (300 MHz, $CHCl_3$, peak assignments were done on a basis of 2D COSY spectra): δ 8.55 (s, 8H, β- pyrrole), 8.19 (m, 8H, *m*-Ph), 7.67 (m, 12H, *o*-Ph, *p*-Ph), 7.65 (d, 4H, $H^{4,8}$, $C_{10}H_7NC$, $^3J_{H\text{-}H}$ = 10 Hz), 7.32 (t, 2H, H^6, $C_{10}H_7NC$, $^3J_{H\text{-}H}$ = 10 Hz), 6.91 (t, $H^{5,7}$, $C_{10}H_7NC$, $^3J_{H\text{-}H}$ = 10 Hz), 5.32 (s, 4H, $H^{1,3}$, $C_{10}H_7NC$) ppm. UV-vis [DCM; λ, (log ε, $M^{-1}cm^{-1}$)]: 417 (5.69), 297 (5.27) nm. IR (KBr),: ν(NC) 2067 cm^{-1}. HRMS (APCI-TOF, positive ions mode): Calculated for $C_{66}H_{42}N_6Ru$: 1020.2527; Found: 1020.2520 $[M]^+$.

Synthesis of (6-CNAz)$_2$RuTPP. Commercially available (OC)RuTPP (0.10 g, 0.13 mmol) was added to a solution of the 6-CNAz ligand (0.15 g, 0.99 mmol) in 50 mL of the toluene: DCM (1/1, v/v) mixture under argon atmosphere. The reaction mixture was stirred for 2 h at room temperature. The solvent was then removed under the reduced pressure. The resulting solid was washed several times with benzene-hexanes and hexanes and dried under vacuum. Yield: 0.13 g (65 %). Elemental analysis: calculated for $C_{66}H_{42}N_6Ru \cdot C_6H_6$: C, 78.74; H, 4.40; N, 7.65. Found: C, 78.39; H, 4.67; N, 7.74. ^{1}H NMR (300 MHz, $CHCl_3$, peak assignments were done on a basis of 2D COSY spectra): δ 8.58 (s, 8H, β- pyrrole), 8.18 (m, 8H, *m*-Ph), 7.66 (m, 12H, *o*-Ph, *p*-Ph), 7.63 (t, H^2, $C_{10}H_7NC$, $^3J_{H\text{-}H}$ = 10 Hz), 7.40 (d, 4H, $H^{4,8}$, $C_{10}H_7NC$, $^3J_{H\text{-}H}$ = 10 Hz), 7.04 (d, 4H, $H^{1,3}$, $C_{10}H_7NC$, $^3J_{H\text{-}H}$ = 10 Hz), 4.59 (d, 4H, $H^{5,7}$, $C_{10}H_7NC$, $^3J_{H\text{-}H}$ = 10 Hz). UV-vis [DCM; λ, (log ε, $M^{-1}cm^{-1}$)]: 417 (5.35), 297 (4.93) nm. IR (KBr),: ν(CN) 2061 cm^{-1} (NC). HRMS (APCI-TOF, positive ions mode): Calculated for $C_{66}H_{42}N_6Ru$: 1020.2527; Found: 1020.2525 $[M]^+$.

Instrumentation

A Bruker NMR instrument was used to acquire ^{1}H and 2D COSY NMR spectra at 300 MHz frequency for protons. The ^{1}H NMR spectra are referenced to the corresponding resonances of $CHCl_3$ as internal standard and the chemical shifts are reported in parts per million (ppm). All UV-Vis data were obtained on a JASCO-720 spectrophotometer at room temperature. Jasco V-1500 and OLIS DCM 17 CD spectropolarimeter with a 1.1 T electro- or 1.4 T DeSa permanent magnet were used to obtain all Magnetic Circular Dichroism (MCD) data. The FTIR data were obtained on a Perkin Elmer FTIR-Spectrometer Spectrum 100 at room temperature with solid samples dispersed in KBr pellets. Electrochemical measurements were conducted using a CHI-620C electrochemical analyzer employing the three-electrode scheme. Carbon or platinum working, platinum auxiliary and Ag/AgCl pseudo-reference electrodes were used in a 0.05 M solution of TBAF in DCM. The redox potentials are referenced to the FcH/FcH^{+} couple using decamethylferrocene as internal standard. Spectroelectrochemical data were collected using a custom-made 1 mm cell, a working electrode made of platinum mesh, and a 0.15 M solution of TBAF in DCM. High-resolution APCI mass spectra were recorded using a Bruker MicrOTOF-III system for samples dissolved in in THF. Elemental analysis was performed by Atlantic Microlab, Inc. in Atlanta, Georgia.

Computational Details

All computations were performed using the *Gaussian 09* software package running under UNIX OS.[13] Molecular orbital contributions were compiled from single point calculations using the QMForge program.[14] All geometries were optimized using B3LYP exchange-correlation functional and full-electron double-ζ quality basis set (DGDZVP) for all atoms. Frequencies were

calculated for all optimized geometries in order to ensure that final geometries represent minima on potential energy surface. In all single-point calculations, the M06 exchange-correlation functional[15] was used. Time Dependent Density Functional Theory (TDDFT) calculations were conducted for the first 80 excited states in order to ensure that all charge transfer (CT) and $\pi-\pi^*$ transitions of interest were accounted for. Solvent effects were modelled using polarized continuum model (PCM) approach.

X-ray crystallography

Single crystals of $(2\text{-CNAz})_2$RuTPP and $(6\text{-CNAz})_2$RuTPP suitable for X-ray crystallographic analysis were obtained by slow evaporation from their toluene solutions. X-ray diffraction data were collected on Rigaku RAPID II Image Plate system using graphite-monochromated radiation. Experimental data collection, cell refinement, reduction and absorption correction were performed by CrystalClear-SM Expert 2.0 r12.[1] The structures were solved by Superflip.[2] The toluene solvent molecule in the X-ray structure of the $(2\text{-CNAz})_2$RuTPP complex was found to be severely disordered and thus was removed using the *PLATON SQUEEZE* procedure. All hydrogen atoms were placed in their geometrically expected positions. The isotropic thermal parameters of all hydrogen atoms were fixed to the values of the equivalent isotropic thermal parameters of the corresponding carbon atoms using riding model constraints so that $U_{iso}(H) = 1.2U_{eq}(C)$ for the hydrogen atoms. Both structures reported herein were completely refined via the full-matrix least square method using the *Crystals for Windows* or SHELXTL program.[25] Complete crystallographic information is available in the CIF accompanying this article. CCDC 1902219 and 1902218 contain the supplementary crystallographic data for all compounds. These data can be obtained free of charge via www.ccdc.cam.ac.uk/conts/retrieving.html (or from Cambridge

Crystallographic Data Centre, 12 Union Road, Cambridge CB2 1EZ, UK; fax: (+44) 1223-336-033 or deposit@ccdc.cam.ac.uk).

Crystal data for $(6\text{-CNAz})_2$RuTPP: FW 1020.12, MoKα radiation (λ = 0.71073 Å) at 123 K, monoclinic, space group C2/c, a = 23.455(2), b = 12.6158(8), c = 19.111(3) Å, α = 90 °, β = 111.223(9) °, γ = 90°, V = 5271.6(10) $Å^3$, Z = 4, μ = 0.345mm^{-1}, 9405 reflections, (2982 I > 2.0/s(I)), parameters 715, θ_{max} = 25.027; final R_1 = 0.0711, R_w = 0.1950. Toluene solvent molecule was removed using the program PLATON SQUEEZE.[3] The structure was refined by full-matrix least-squares refinement on F^2 using SHELXL-2014/7[4] and the user interface ShelXle.[5] Additional crystallographic information may be found in the cif, CCDC-1902218.

Crystal data for $(2\text{-CNAz})_2$RuTPP: FW 1020.31, CuKα radiation (λ = 1.54187 Å) at 123 K, monoclinic, space group $P2_1/c$, a = 23.4732(17), b = 12.9276(2), c = 19.052(4) Å, α = 90 °, β = 112.963(8) °, γ = 90°, V = 5323.2(11) $Å^3$, Z = 4, μ = 2.790 mm^{-1}, 9485 reflections, (3734 I > 2.0/s(I)), parameters 330, θ_{max} = 68.246; Final R_1 = 0.1044 [I>2\σ(I)], R_w = 0.3674 [I>-3.0\σ (I)]. The structure was refined by full-matrix least-squares refinement on F^2 using CRYSTALS.[6] Additional crystallographic information may be found in the cif, CCDC-1902219

Results and Discussion

Synthesis, Spectroscopy, and X-ray structures. The isocyanoazulene $(2\text{-CNAz})_2$RuTPP and $(6\text{-CNAz})_2$RuTPP complexes were synthesized using a simple coordination reaction shown in Scheme 1.

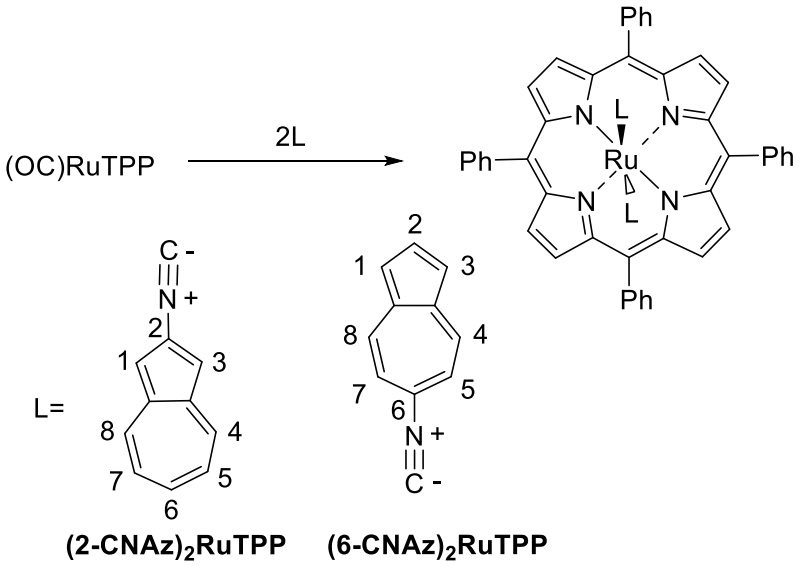

Scheme 1. Synthetic strategy for preparation of the $(RNC)_2RuTPP$ complexes.

The "reference" $(t\text{-BuNC})_2RuTPP$ complex was synthesized and purified according to the literature procedure.[10] Similar to the ^1H NMR patterns documented for other axially coordinated diamagnetic ruthenium / iron porphyrins and phthalocyanines,[17] the ^1H NMR resonances corresponding to the axial ligands (i.e., isocyanoazulenes) in $(2\text{-CNAz})_2RuTPP$ and $(6\text{-CNAz})_2RuTPP$ are shifted significantly upfield compared to the corresponding free ligands. Both species show the same number of resonances with four signals attributable to the porphyrin macrocycle, (thereby indicating a pseudo D_{4h} symmetry with free rotation about the C-Ru-C axis) and four signals corresponding to two equivalent azulenyl moieties Notably, the ^1H NMR signatures of the tetraphenylporphyrin cores in $(2\text{-CNAz})_2RuTPP$ and $(6\text{-CNAz})_2RuTPP$ are very similar to those previously reported for other RuTPP complexes.[7]

The ^1H NMR patterns for the axial isocyanoazulene ligands are markedly different for the two isomers. For complex $(2\text{-CNAz})_2RuTPP$, the ^1H NMR resonance for the H-atoms at 1,3-positions of the azulenic scaffold ($H^{1,3}$) is shifted -2.43 ppm (upfield), whereas the $H^{5,7}$ signal is

shifted -1.1 ppm (upfield), compared to the corresponding resonances documented for the $H^{1,3}$ and $H^{5,7}$ nuclei of the free 2-CNAz ligand. The relatively large upfield shift of the $H^{1,3}$ resonance is consistent with the closer proximity of these azulenic H-atoms to the porphyrin ring. For (6-CNAz)$_2$RuTPP complex, the situation is reversed. Indeed, the ^{1}H NMR signal for the $H^{1,3}$ nuclei is shifted -0.82 ppm, whereas that for the $H^{5,7}$ nuclei is shifted -3.19 ppm, compared to the corresponding resonances recorded for the free 6-CNAz ligand In agreement with the previous argument, now the $H^{5,7}$ azulenic atoms in (6-CNAz)$_2$RuTPP are positioned closer to the porphyrin ring and, therefore, exhibit a larger upfield shift of the corresponding ^{1}H NMR resonances than the $H^{1,3}$ environment. Moreover, the ^{1}H NMR resonance for the $H^{5,7}$ atoms of 6-CNAz undergoes a greater upfield shift (-3.19 ppm) upon coordination to form (6-CNAz)$_2$RuTPP than the upfield shift (-2.43 ppm) of the ^{1}H NMR signal for the $H^{1,3}$ atoms of 2-CNAz upon coordination of the latter to form (2-CNAz)$_2$RuTPP. This observation is consistent with the azulenic $H^{5,7}$ atoms in (6-CNAz)$_2$RuTPP complex being closer to the porphyrin ring as compared to the azulenic $H^{1,3}$ atoms in (2-CNAz)$_2$RuTPP complex. The single crystal X-ray structural analyses of (2-CNAz)$_2$RuTPP and (6-CNAz)$_2$RuTPP confirm the above statement (*vide infra*). The C≡N stretching vibrations (ν_{CN}) of the isocyano junctions in (2-CNAz)$_2$RuTPP and (6-CNAz)$_2$RuTPP complexes occur at 2067 cm^{-1} and 2061 cm^{-1}, respectively. Notably, the ν_{CN} bands in the IR spectra of the free 2-CNAz and 6-CNAz ligands are at 2118 cm^{-1} and 2111 cm^{-1}, respectively.[8] The lowering of the energies of ν_{CN} upon coordination of 2-CNAz or 6-CNAz to RuTPP are nearly identical (51 cm^{-1} vs. 50 cm^{-1}) and signify appreciable Ru(dπ) $\rightarrow$ CNAz(pπ*) backbonding interactions in (2-CNAz)$_2$RuTPP and (6-CNAz)$_2$RuTPP complexes. The APCI mass spectra of (2-CNAz)$_2$RuTPP and (6-CNAz)$_2$RuTPP are illustrated in Supporting Information Figure Sx and confirm the 2:1 isocyanoazulene / ruthenium porphyrin core stochiometry in these adducts.

The UV-vis and MCD spectra of the complexes (2-CNAz)$_2$RuTPP and (6-CNAz)$_2$RuTPP are shown in Figure 1. As in the case of our previously reported (RNC)$_2$RuTPP complexes,[18] the UV-vis and MCD spectra of (2-CNAz)$_2$RuTPP and (6-CNAz)$_2$RuTPP presented in this article are superposition of the spectra of RuTPP and axial ligands. In particular, since the intensities and energies of the π–π* transitions of both azulenes and TPP fragments in the *Q*-band region are similar, UV-vis spectra of **1** and **2** are much less defined compared to the reference (*t*-BuNC)$_2$RuTPP in which clear $Q_{0\text{-}0}$ and $Q_{0\text{-}1}$ bands were observed at 582 and 529 nm (Supporting Information). However, since MCD intensities of Faraday *B*-terms of the axially coordinated isocyanoazulenes are incomparably smaller that the *A*-term intensities of the $Q_{0\text{-}0}$ and $Q_{0\text{-}1}$ bands of TPP core, MCD spectroscopy allows clear identification of the $Q_{0\text{-}0}$ band at 582 ((2-CNAz)$_2$RuTPP) or 596 ((6-CNAz)$_2$RuTPP) nm and $Q_{0\text{-}1}$ band at 538 ((2-CNAz)$_2$RuTPP) and 541 ((6-CNAz)$_2$RuTPP) nm (Figure 1). As expected for the effective four-fold symmetry of the porphyrin core in the (CNAz)$_2$RuTPP complexes, ΔHOMO > ΔLUMO (ΔHOMO is the energy difference between two highest energy, TPP-centered π-orbitals and ΔLUMO is the energy difference between two lowest energy, TPP-centered π∗-orbitals), which is reflected in negative-to-positive (in ascending energy) sequence of the MCD signals.[19] The Soret band region in the electronic spectra of the (CNAz)$_2$RuTPP complexes is dominated by a single Soret band observed at *ca.* 417 nm, which is associated with a very intense Faraday *A*-term in the respective MCD spectra (Figure 1).[20]

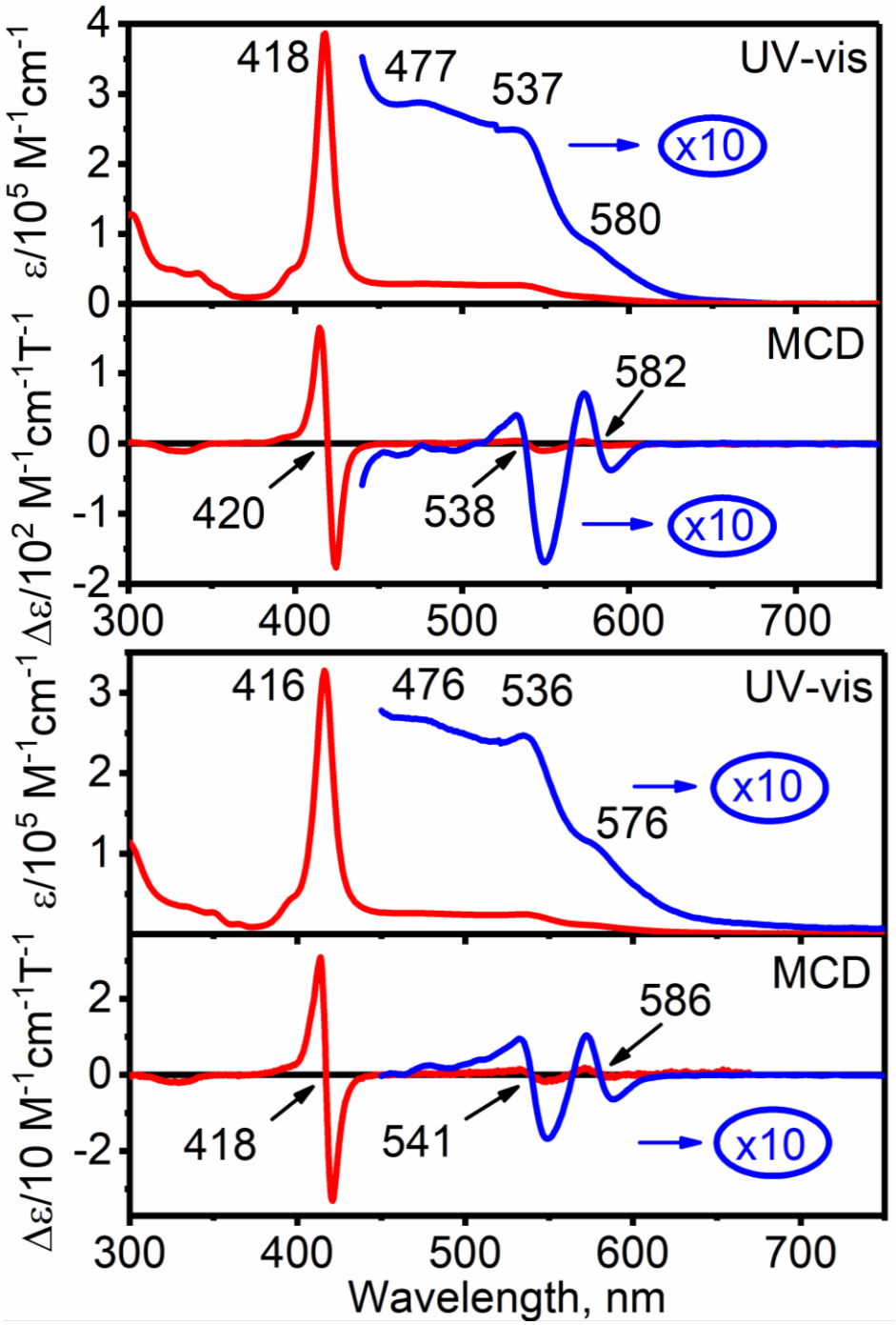

Figure 1. Experimental UV-vis and MCD spectra of $(2\text{-CNAz})_2$RuTPP(top) and $(6\text{-CNAz})_2$RuTPP (bottom).

The molecular structures of $(2\text{-CNAz})_2$RuTPP and $(6\text{-CNAz})_2$RuTPP complexes were determined by single crystal X-ray crystallography. Slow evaporation of a toluene solution of $(2\text{-CNAz})_2$RuTPP or $(6\text{-CNAz})_2$RuTPP at room temperature provided crystals suitable for X-ray

analysis. $(2\text{-CNAz})_2$RuTPP and $(6\text{-CNAz})_2$RuTPP complexes co-crystalized with one toluene molecule in the asymmetric unit. Platon Squeeze[21] was used to remove the badly disordered toluene in the structure of $(6\text{-CNAz})_2$RuTPP. The crystal sizes were quite small, which resulted in a limited resolution of 0.90 Å and 0.84 Å, respectively. The ORTEP diagrams of $(2\text{-CNAz})_2$RuTPP and $(6\text{-CNAz})_2$RuTPP are displayed in Figure 2. Despite the low resolution of the X-ray structure for $(2\text{-CNAz})_2$RuTPP complex, the structural differences between the isolated isomeric $(2\text{-CNAz})_2$RuTPP and $(6\text{-CNAz})_2$RuTPP complexes can be readily appreciated.

$(2\text{-CNAz})_2$RuTPP complex crystalizes in the space group $P2_{1/c}$ and $(6\text{-CNAz})_2$RuTPP complex crystallized in the space group C2/c. The ruthenium ion in $(6\text{-CNAz})_2$RuTPP complex is located on an inversion center resulting in one-half of the molecule being crystallographically unique. The Ru atom sits in the plane of the porphyrin ring in both complexes. In both $(2\text{-CNAz})_2$RuTPP and $(6\text{-CNAz})_2$RuTPP, the ruthenium atom features a slightly compressed tetragonal environment. Consistent with the metric data reported earlier for the Ru-porphyrin-isocyanide complexes, the Ru-N bond length is about 0.08 Å longer than the Ru-C distances.[22] The Ru-C distances of 1.98-1.99 Å observed in $(2\text{-CNAz})_2$RuTPP and $(6\text{-CNAz})_2$RuTPP complexes are very similar to the those previously reported for the Ru-porphyrin complexes with isocyanoarene and isocyanoferrocene axial ligands.[22] The isonitrile C≡N bond distances in $(2\text{-CNAz})_2$RuTPP and $(6\text{-CNAz})_2$RuTPP (1.15-1.17 Å) suggest a modest extent of Ru(dπ) → CNAz(pπ*) backbonding.[22]

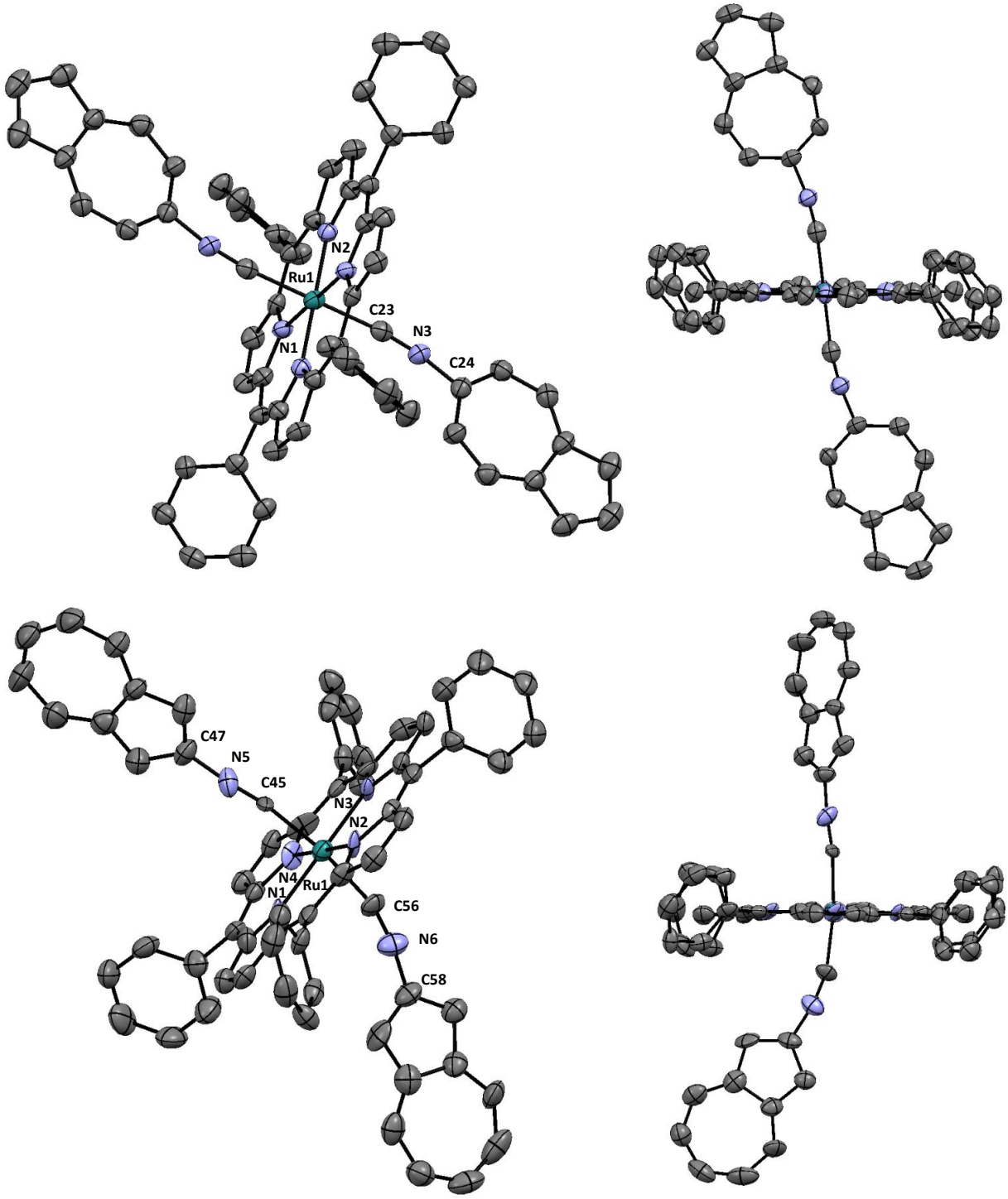
N2
Ru1
C23
N3
N1
C24
C47
N5
C45
N3
N2
N4
N1
Ru1
C56
N6
C58

Figure 2. Molecular structures of $(2\text{-CNAz})_2$RuTPP (left) and $(6\text{-CNAz})_2$RuTPP (right) as 50% thermal ellipsoids. All hydrogen atoms are omitted for clarity, as are the toluene solvent molecules of crystallization observed in the unit cells of both $(2\text{-CNAz})_2$RuTPP and $(6\text{-CNAz})_2$RuTPP. Carbon atoms are green, nitrogen atoms are blue, and ruthenium atoms are grey. Selected bond distances (Å) and angles (°): $(6\text{-CNAz})_2$RuTPP Ru1-C23 1.980(7), Ru1-N1 2.064(5), Ru1-N2 2.054(5), N3-C23 1.169(7), N3-C24 1.411(7), C23-Ru1-C23 180.0, C23-N3-C24 171.3(6), N3-C23-Ru1 171.3(5); $(2\text{-CNAz})_2$RuTPP: Ru1-N1 2.095(11), Ru1-N2 2.071(10), Ru1-N3 2.103(10), Ru1-N4 2.063(9), Ru1-C45 1.999(11), Ru1-C56 1.995(13), N5- C45 1.150(16), N5-C47 1.391(17), N6-C56 1.167(17), N6-C58 1.382(18), C45-Ru1-C56 172.1(6), C45-N5-C47 173.4(15), C56-N6-C58 169.3(16), Ru1-C56-N6 164.0(14), Ru1-C45-N5 171.6(11), C45-N5-C47 173.4(15), C56-N6-C58 169.3(16)

Redox Properties. The redox properties of the azulene containing porphyrins $(2\text{-CNAz})_2$RuTPP and $(6\text{-CNAz})_2$RuTPP complexes were investigated by the electrochemical and spectroelectrochemical approaches. The typical cyclic voltammetry (CV) and differential pulse voltammetry (DPV) of two isomers are shown in Figure 3 and numerically in Table 1. In both cases the first oxidation has been assigned to Ru^{II}/Ru^{III} redox couple based on the redox potential, spectroelectrochemical data, and previously reported for similar $[(RNC)_2RuTPP]^+$ complexes EPR spectra. Similar to the $(RNC)_2$RuTPP systems, the Ru^{II}/Ru^{III} oxidation potential slightly depends on the nature of the axial ligand. For instance, the $(6\text{-CNAz})_2$RuTPP complex has about 40 mV higher oxidation potential compared to the $(2\text{-CNAz})_2$RuTPP complex. The second reversible oxidation wave in $(2\text{-CNAz})_2$RuTPP observed at 740 mV was assigned to the oxidation of the porphyrin core, while two closely spaced irreversible processes observed at 1.14 and 1.27 V were assigned to the oxidation the axial isocyanoazulene ligands (irreversible oxidation of the free 2-

isocyanoazulene was observed at 0.92 V). In the case of (6-CNAz)$_2$RuTPP, however, the irreversible oxidation potentials of axial isonitrile ligands was found to be close to the reversible oxidation potential of porphyrin and thus the second wave observed in the electrochemical experiments consists of three closely spaced electrochemical events. Two clearly observed in DCM/0.05 M TBAF system irreversible oxidation processes at the axial ligands in (2-CNAz)$_2$RuTPP allowed us to estimate comproportionation constant for the formation of the mixed-valence [(2-CNAz)$_2$RuTPP]$^{3+}$ complex (K_c = 159). However, since axial ligand oxidation is irreversible in nature, we were not able to collect any spectroscopic data on such a mixed-valence species. Electrochemical experiments are suggestive of two closely spaced partially reversible reductions observed in (CNAz)$_2$RuTPP complexes (Figure 3). Based on the closeness of observed potentials to those of free isocyanoazulenes (Table 1), we assigned both processes to the sequential reduction of the axial ligands. Although not surprising, such behaviour is in a stark contrast with the other L$_2$RuTPP complexes in which the only porphyrin-centred reduction processes were

observed.

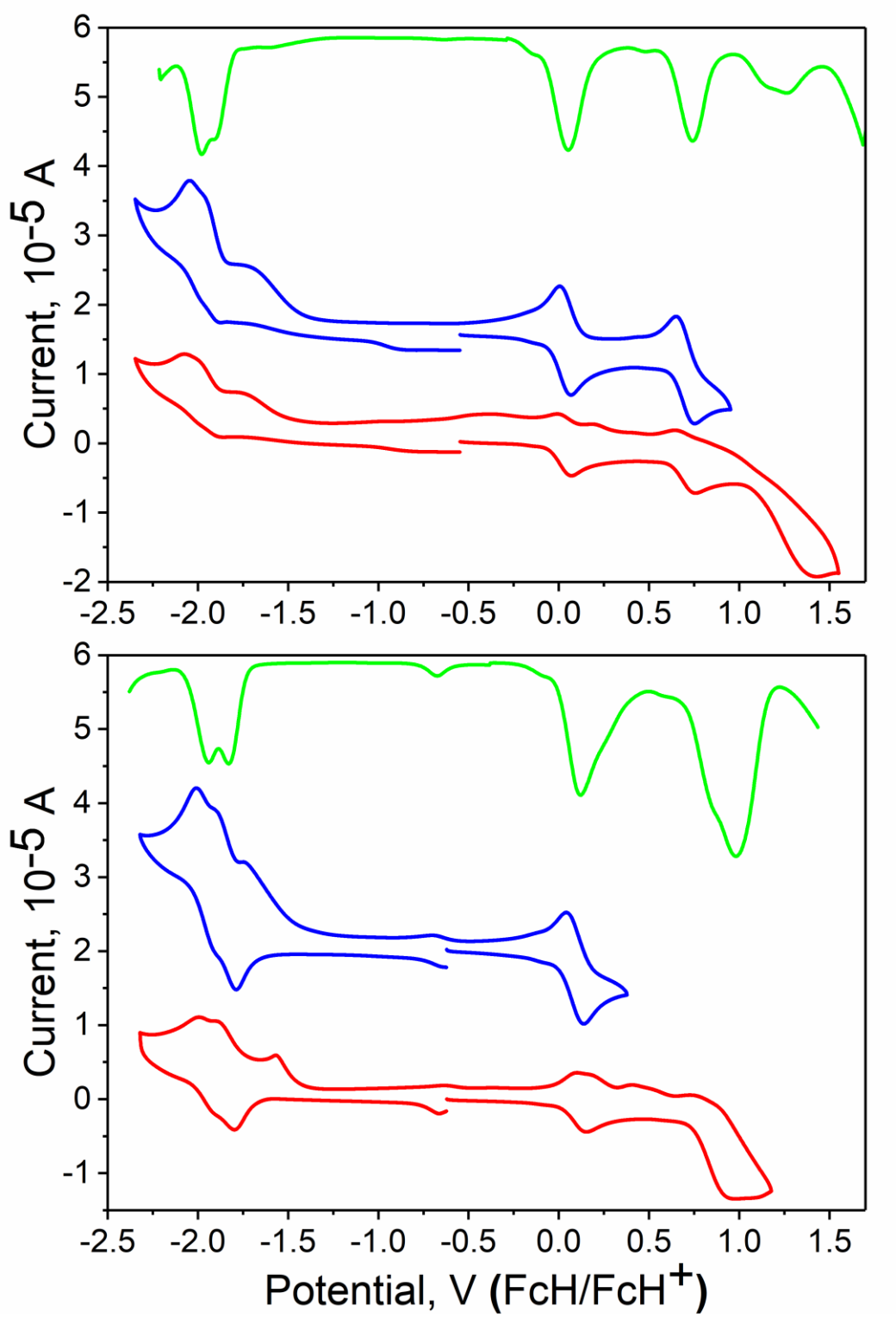
Current, 10-5 A
6
5
4
3
2
1
0
-1
-2
-2.5
-2.0
-1.5
-1.0
-0.5
0.0
0.5
1.0
1.5
Current, 10-5 A
Potential, V (FcH/FcH+)

Figure 3. DPV (red) and CV (blue) electrochemical data for $(2\text{-CNAz})_2$RuTPP (top) and $(6\text{-CNAz})_2$RuTPP complexs in DCM/0.05 M TBAF solution.

Table 1. Oxidation potentials (V) for $(RNC)_2$RuTPP complexes determined by electrochemical experiments in DCM/0.05M TBAF system at room temperature.[a]

Complex	Ru^{II}/Ru^{III}	TPP^{2-}/TPP^{-}	$2L/2L^{+}$	$2L^{+}/2L^{2+}$	$2L/2L^{-}$	$2L^{-}/2L^{2-}$
$(2\text{-CNAz})_2$RuTPP	0.05	0.74	1.14[d]	1.27[d]	-1.91[d]	-1.98[d]
$(6\text{-CNAz})_2$RuTPP	0.09	0.84[e]	0.98[d,e]	0.98[d,e]	-1.83[d]	-1.94[d]
$(t\text{-BuNC})_2$RuTPP[b]	-0.023	0.713				
$(FcNC)_2$RuTPP[b]	0.033	0.997	0.437	0.533		
2CNAz[c]			0.92[d]		-1.80[d]	
6CNAz[c]					-1.79	

[a] All potentials are referenced to the FcH/FcH^{+} couple and are ± 10 mV; [b] ref. xx; [c] ref xx; [d] irreversible or partially reversible; [e] three single-electron, closely spaced oxidation waves.

In order to confirm the tentative assignments of oxidation waves observed in electrochemical experiments we have conducted spectroelectrochemical measurements on both isocyanoazulene systems. During the first oxidation process under spectroelectrochemical conditions, the Soret band undergoes reduction in intensity by ~60% and higher energy shift to 396-397 nm. In the *Q*-band region, upon the first oxidation process, three new bands at ~570, 644, and ~715 nm appear in the UV-vis spectra of $[(2\text{-CNAz})_2\text{RuTPP}]^{+}$ and $[(6\text{-CNAz})_2\text{RuTPP}]^{+}$ (Figures 4 and 5). Similar transformation has already been observed in the case of the Ru porphyrins axially coordinated with similar isocyanide ligands and is very characteristic of the

formation of Ru^{III} porphyrins. Because of the closeness of the porphyrin and azulene oxidation potentials in $(6\text{-CNAz})_2$RuTPP, we did not pursue further oxidation of $[(6\text{-CNAz})_2\text{RuTPP}]^+$ to $[(6\text{-CNAz})_2\text{RuTPP}]^{2+}$. However, in the case of (2-CNAz)2RuTPP complex, the first and the second oxidation potentials are well-separated and thus, we were able to further oxidize $[(2\text{-CNAz})_2\text{RuTPP}]^+$ complex to $[(2\text{-CNAz})_2\text{RuTPP}]^{2+}$ (Figure 4). During the second oxidation step, the intensity of the Soret band at 397 nm decreases and the formation of new bands at 578, 639, 734, and ~850 nm has been observed in UV-Vis-NIR spectra. The formation of broad, low intensity bands around 850 nm is a very characteristic indicator of the formation of delocalized porphyrin cation-radical. We also were able to confirm the first oxidation process using chemical oxidation experiments with "magic blue" as an oxidant (Supporting Information). The observed changes in the UV-vis spectra of the $(2\text{-CNAz})_2$RuTPP and $(6\text{-CNAz})_2$RuTPP complexes correlate well with spectroelectrochemical data and are suggestive of the Ru^{II}/Ru^{III} oxidation process. Overall the spectroelectrochemical and chemical oxidation data confirms our tentative electrochemical assignments and correlate well with the previous reports on ruthenium(II) tetraphenylporphyrin complexes axially coordinated with the organic isocyanides.

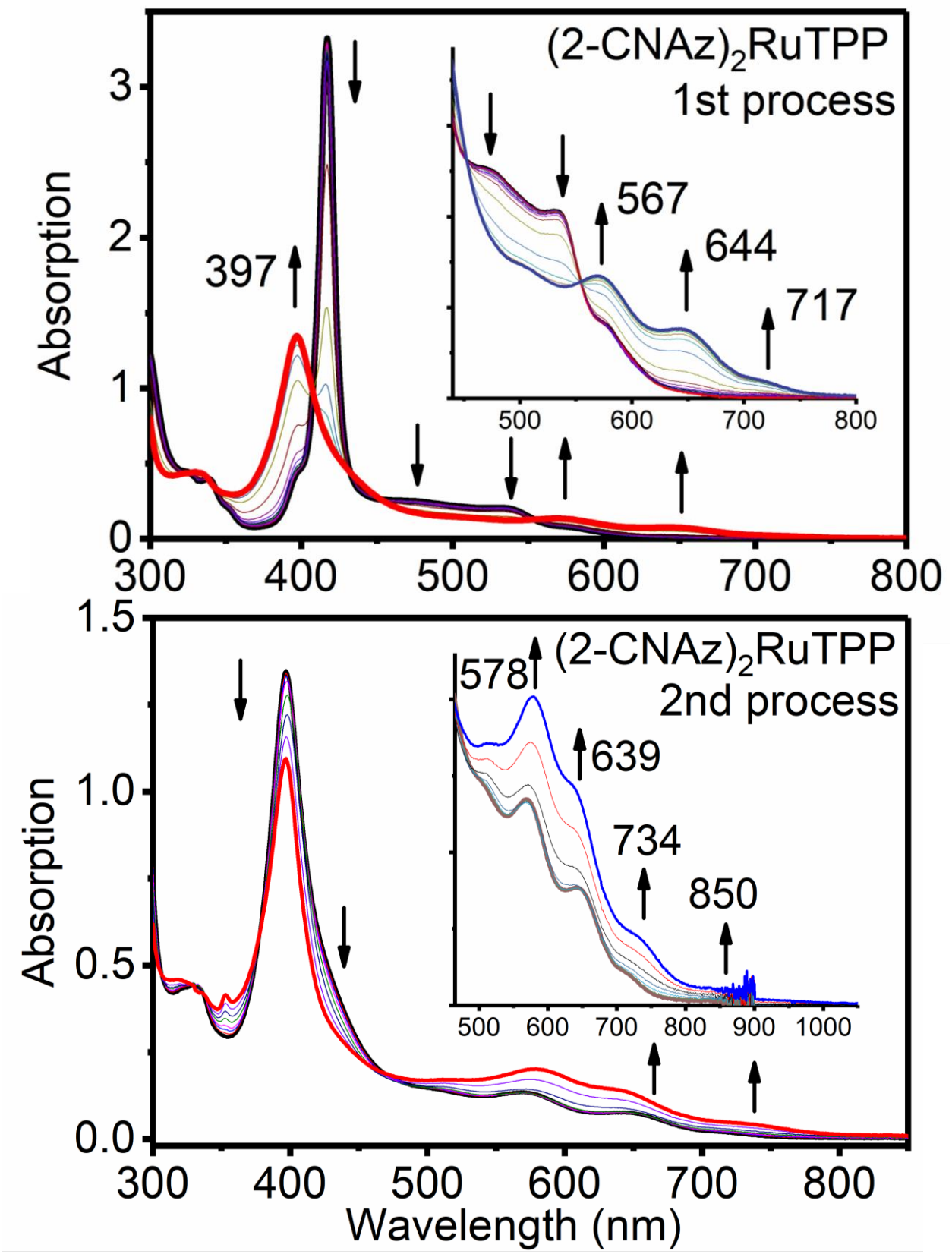
(2-CNAz)2RuTPP
1st process
397
567
644
717
Absorption
(2-CNAz)2RuTPP
2nd process
578
639
734
850
Absorption
Wavelength (nm)

Figure 4. Spectroelectochemical oxidation of the (2-CNAz)$_2$RuTPP complex in DCM/0.15M TBAF system at room temperature.

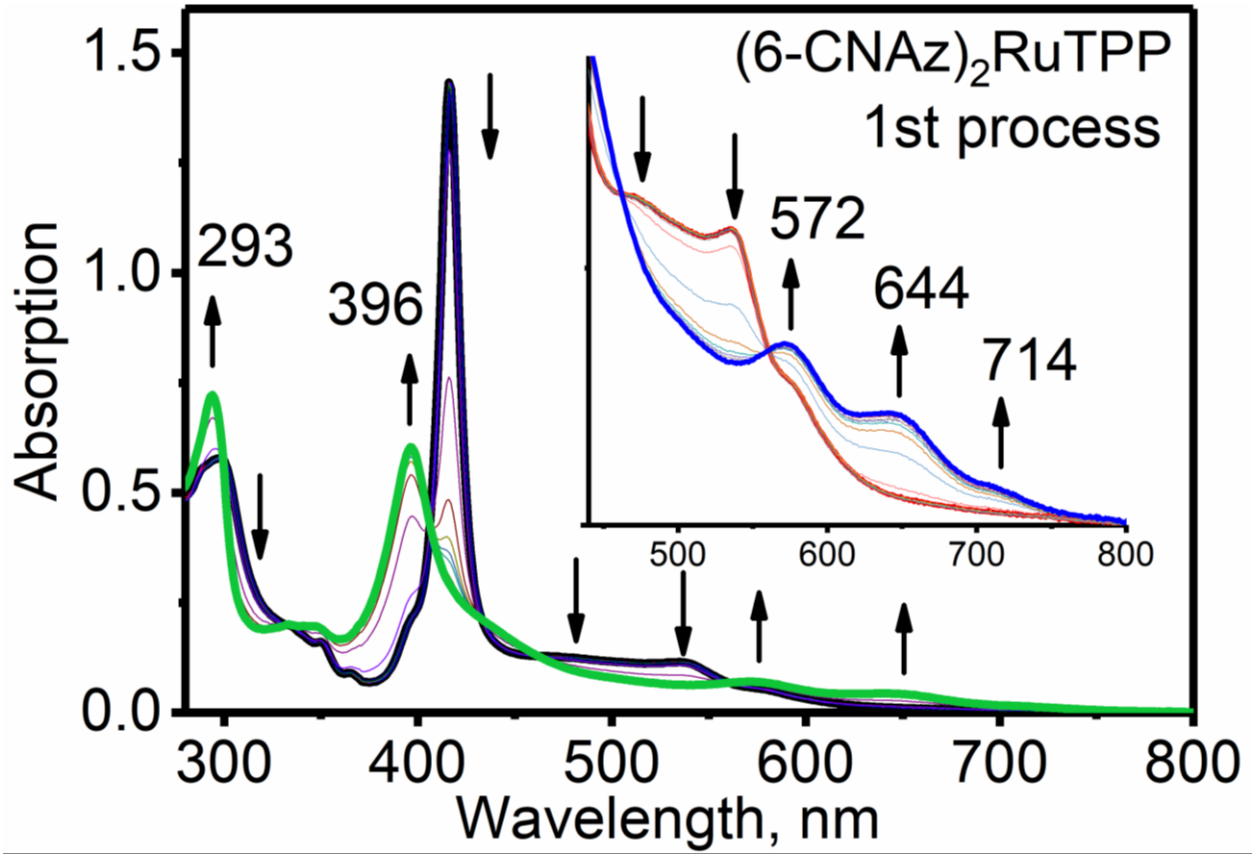

Figure 5. Spectroelectochemical oxidation of the (6-CNAz)$_2$RuTPP complex in DCM/0.15M TBAF system at room temperature.

DFT and TDDFT Calculations. The DFT-predicted frontier molecular orbitals energy diagrams and molecular orbital compositions for (2-CNAz)$_2$RuTPP and (6-CNAz)$_2$RuTPP complexes, are shown in Figures 6, 7 and Table 2. The choice of the M06 exchange-correlation functional for energy and excited states calculations was dictated by the best agreement between the theory and experiment obtained in the TDDFT calculations although the other tested exchange-correlation functionals (BP86, TPSSh, B3LYP, CAM-B3LYP, M06L, M11, MN12SX, and M11L) predict qualitatevely siilar electronic structures of the target copounds. The large contribution of Hartree-Fock exchange part in this exchange correlation functional, however, resulted in a relatively strong

stabilization of the metal-centered orbitals compared to the porphyrin π orbitals. Indeed, in the case of the (2-CNAz)$_2$RuTPP and (6-CNAz)$_2$RuTPP complexes, the HOMO and HOMO-1 were predicted to be porphyrin centered MOs followed by the predominantly Ru-centered d_π molecular orbitals (HOMO-2 and HOMO-3). The difference between TPP-centered HOMO and Ru-centered HOMO-2 was predicted to be about 0.4 eV in energy. In both complexes, DFT predict predominantly ruthenium-centered d_{xy} orbital as HOMO-6. In addition, the azulene-centered occupied molecular orbitals were found to be the HOMO-4 and HOMO-5 in both complexes. The M06 calculations correctly predict that the LUMO and LUMO+1 orbitals in the (2-CNAz)$_2$RuTPP and (6-CNAz)$_2$RuTPP complexes are azulene-centered, while classic Gouterman's porphyrin-centered orbitals should be the LUMO+2 and LUMO+3. Although electrochemical experiments discussed below suggestive of the first Ru-centered oxidation, all tested exchange-correlation functionals still predicts the HOMO to be porphyrin-centered. In order to overcome such a discrepancy between theory and experiment, we conducted CASSCF calculations on our systems, which will be discussed below. Overall, DFT-predicted electronic structures of the (2-CNAz)$_2$RuTPP and (6-CNAz)$_2$RuTPP complexes suggest that in addition to the classic porphyrin-centered Gouterman's π–π* transitions, the low-energy azulene-centered π–π* transitions, porphyrin(π)-azulene(π*) charge-transfer transitions, Ru(d)-azulene(π*) charge-transfer

transitions, and Ru(d)-porphyrin(π*) charge-transfer transitions might complicate the visible region of the UV-vis spectra of $(2\text{-CNAz})_2$RuTPP and $(6\text{-CNAz})_2$RuTPP complexes.

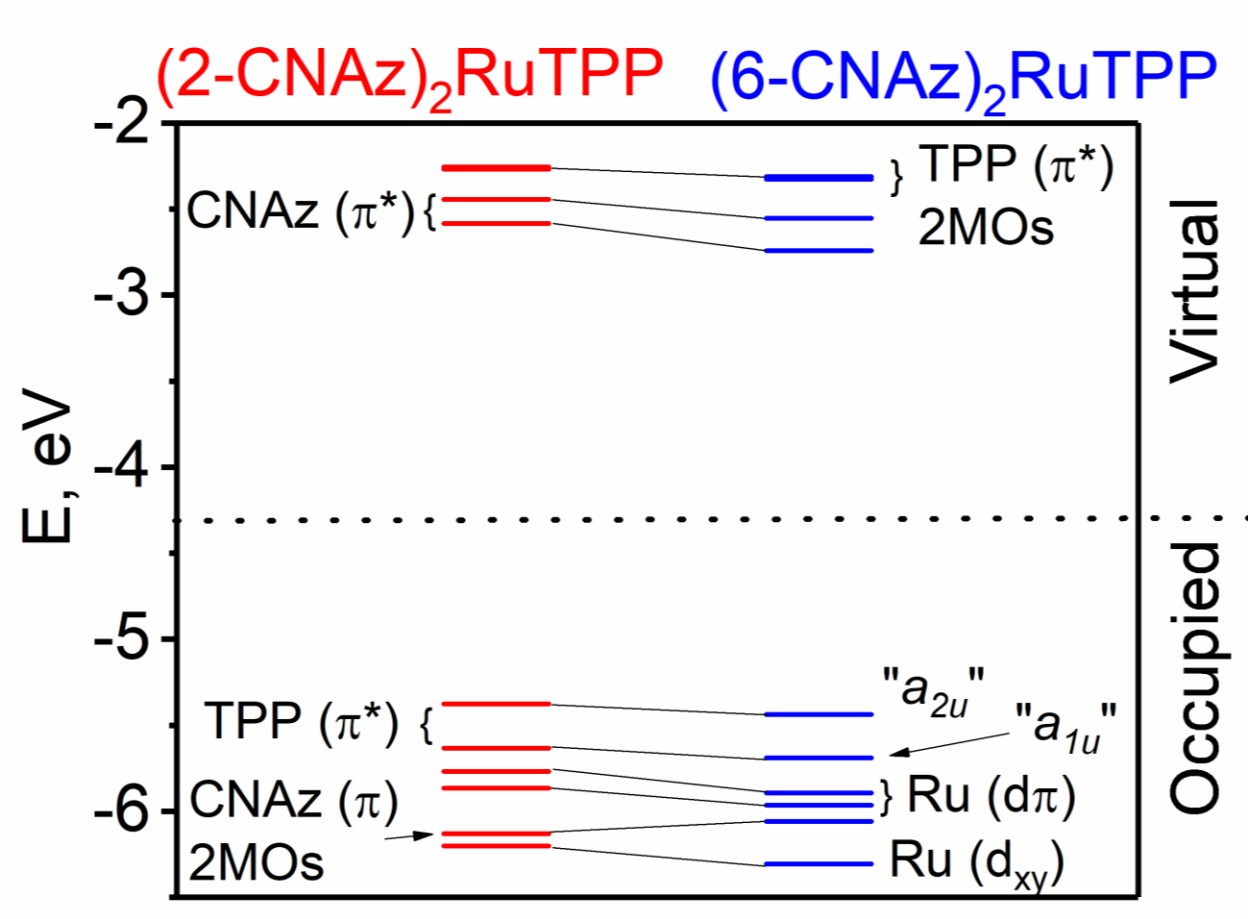

Figure 6. DFT-predicted orbital energy diagrams for $(RNC)_2$RuTPP complexes.

	$(2\text{-CNAz})_2$RuTPP	$(6\text{-CNAz})_2$RuTPP
266_LUMO+3	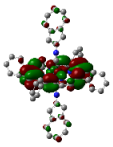	
265_LUMO+2	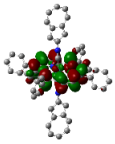	
264_LUMO+1		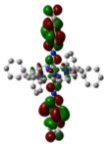
263_LUMO	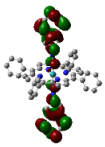	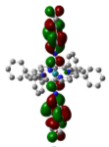
262_HOMO	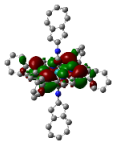	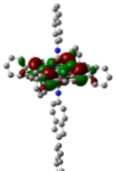
261_HOMO-1	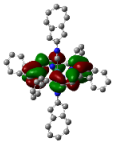	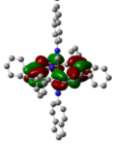
260_HOMO-2		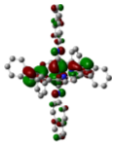
259_HOMO-3	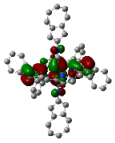	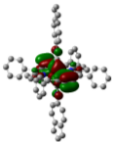
258_HOMO-4	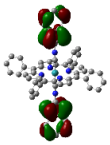	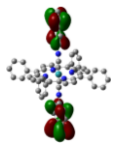
257_HOMO-5	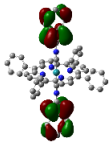	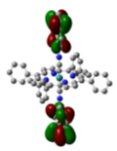
258_HOMO-6	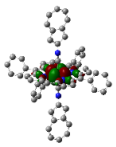	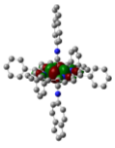

Figure 7. DFT-predicted frontier orbitals for $(RNC)_2RuTPP$ complexes.

Indeed, the TDDFT calculations predict that the porphyrin-centered *Q*-bands that are dominated by the single-electron HOMO, HOMO-1 → LUMO+2, LUMO+3 excitations will be observed around 550 nm (Figure 8). TDDFT calculations also predict several low-energy predominantly azulene-centered HOMO-4, HOMO-5 → LUMO, LUMO+1 transitions in the *Q*-band region with one having comparable intensity to the porphyrin core-centered *Q*-bands. Its TDDFT-predicted energy (528 nm for $(2\text{-CNAz})_2RuTPP$ and 576 nm for $(6\text{-CNAz})_2RuTPP$) follow the trend observed for the free ligands. TDDFT calculations predict several porphyrin (π) → azulene (π^*) transitions in the *Q*-band region, but those should have a very low intensity. In contrary, TDDFT-predicted intensity for the predominant Ru($d\pi$) → azulene (π^*) band (predicted at 483 nm for $(2\text{-CNAz})_2RuTPP$ and 502 nm for $(6\text{-CNAz})_2RuTPP$) is quite large. The most intense bands predicted by TDDFT calculations in azuelene-containing porphyrins were located at 409 nm for both complexes and are dominated by classic Gouterman's porphyrin-centered, HOMO, HOMO-1 → LUMO+2, LUMO+3 single electron excitation. Thus, TDDFT predictions on the UV-Vis spectra on the azuelene containing pophyrins are in a reasonable agreement with the experimental data and explain the broadening of the *Q*-band region in these systems.

Table 2. DFT-predicted molecular orbital compositions in $(RNC)_2RuTPP$ complexes.

$(2\text{-CNAz})_2RuTPP$					
			Composition, %		
MO	Energy (eV)	Symmetry	Ru	Porphyrin	2-CNAz
256	-6.201	a_g	88.84	11.09	0.07
257	-6.129	a_u	0	0.08	99.92
258	-6.129	a_g	0.11	0.2	99.69
259	-5.865	a_g	59.87	34.68	5.45
260	-5.769	a_g	58.37	28.89	12.74
261	-5.634	a_u	0.02	99.97	0.01
262	**-5.377**	$\boldsymbol{a_u}$	**0.29**	**97.49**	**2.22**
263	**-2.583**	$\boldsymbol{a_u}$	**0.92**	**7.15**	**91.93**
264	-2.443	a_g	1.78	12.83	85.39
265	-2.269	a_g	5.07	94.36	0.57
266	-2.255	a_g	6.89	85.54	7.57

$(6\text{-CNAz})_2RuTPP$					
			Composition, %		
MO	Energy (eV)	Symmetry	Ru	Porphyrin	6-CNAz
256	-6.305	a_g	88.85	11.12	0.03
257	-6.059	a_u	0.02	0.15	99.83
258	-6.059	a_g	0	0.08	99.92
259	-5.964	a_g	57.48	34.63	7.89
260	-5.892	a_g	57.39	31.13	11.49
261	-5.69	a_u	0.02	99.95	0.03
262	**-5.438**	$\boldsymbol{a_u}$	**0.28**	**95.75**	**3.97**
263	**-2.742**	$\boldsymbol{a_u}$	**1.26**	**3.87**	**94.87**
264	-2.554	a_g	3.17	8.44	88.39
265	-2.326	a_g	4.89	93.91	1.2
266	-2.312	a_g	7.07	86.59	6.34
282	0.898	Ag	10.13	6.61	83.25

HOMO and LUMO are indicated in bold. Both complexes were optimized in C_i point group.

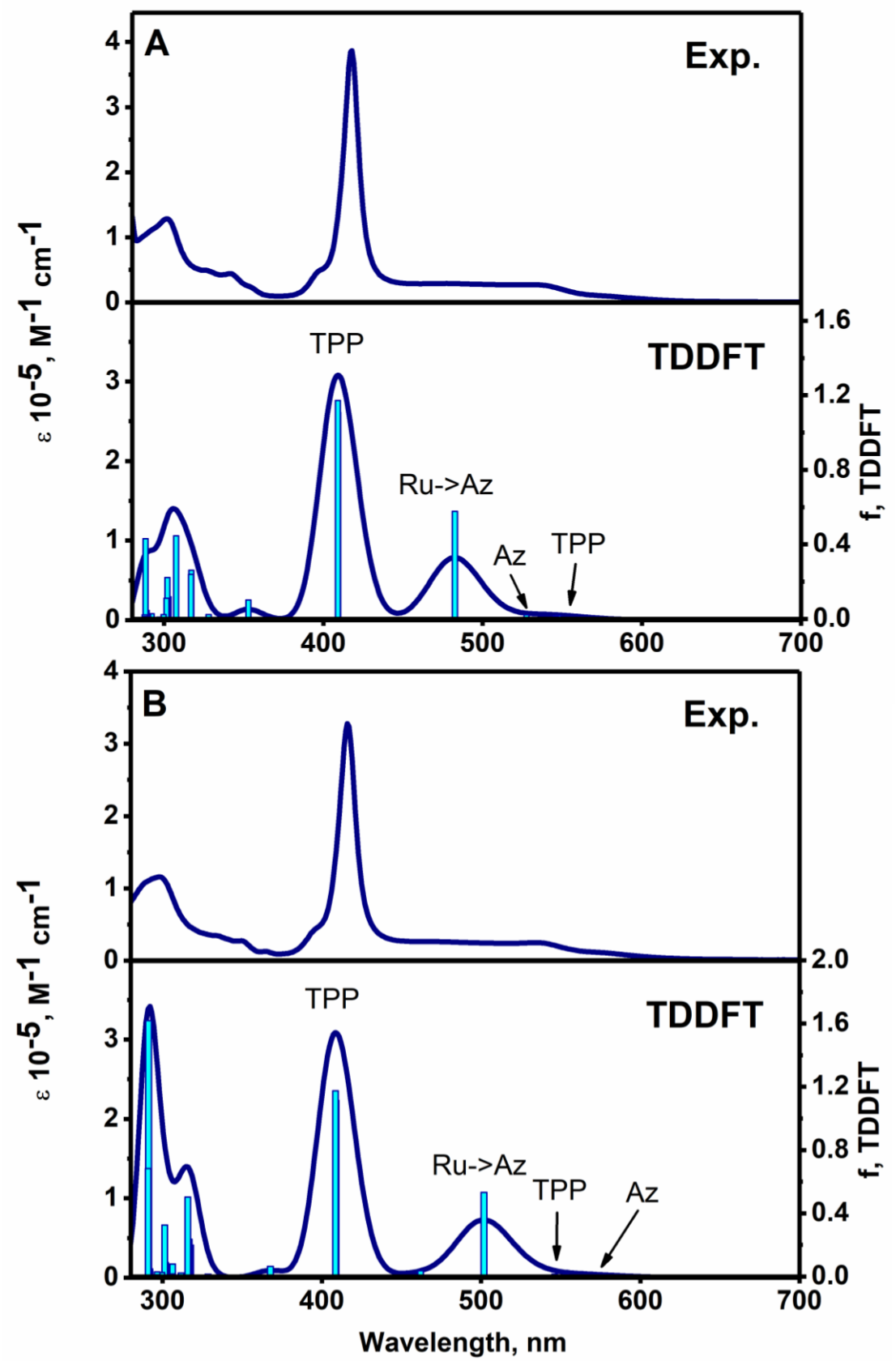
A
Exp.
TDDFT
TPP
Ru->Az
Az
TPP
B
Exp.
TDDFT
TPP
Ru->Az
TPP
Az
ε 10-5, M-1 cm-1
f, TDDFT
Wavelength, nm

Figure 8. Experimental UV-vis (top) and TDDFT predicted (bottom) spectra of (2-CNAz)$_2$RuTPP (**A**), and (6-CNAz)$_2$RuTPP (**B**).

Rashid CASSCF calculations

Conclusions

Two new complexes of the ruthenium(II) tetraphenylporphyrin axially coordinated with two isocyanoazuelenes ((2-CNAz)$_2$RuTPP and (6-CNAz)$_2$RuTPP complexes) were prepared and characterized using UV-vis, MCD, NMR, IR, and ESI-MS spectroscopy as well as X-ray crystallography. The redox properties of the new (2-CNAz)$_2$RuTPP and (6-CNAz)$_2$RuTPP complexes were probed using electrochemical (CV and DPV), spectroelectrochemical, and chemical oxidation methods and correlated to those in published earlier (RNC)$_2$RuTPP compounds. In all cases, the first and second oxidation processes were attributed to the reversible oxidation of the Ru^{II} center, and TPP(2-)/TPP(1-) respectively. Two observed reduction processes were assigned to the stepwise reduction of the axial isocyanoazulene ligands. Spectroelectrochemical and chemical oxidation methods were used to elucidate spectroscopic signature of the $[(RNC)_2RuTPP]^{n+}$ (n = 1,2) species in solution. DFT and TDDFT calculations were used to correlate spectroscopic and redox properties of (2-CNAz)$_2$RuTPP and (6-CNAz)$_2$RuTPP complexes with their electronic structure.

ASSOCIATED CONTENT

Supporting Information

Characterization data for the target porphyrins (Figures S1 – S80); large-size X-ray structures (Figures S81); computational data.

AUTHOR INFORMATION

Corresponding Authors

E-mail: mbarybin@ku.edu

E-mail: Victor.Nemykin@umanitoba.ca

ORCID

Victor Nemykin: 0000-0003-4345-0848

Notes

The authors declare no competing financial interest.

ACKNOWLEDGMENTS

Generous support from the Minnesota Supercomputing Institute, NSERC, CFI, NSF (CHE-1464711 and MRI-0922366), University of Manitoba, and WestGrid Canada to VN, and NSF (CHE-xxxx) to MVB is greatly appreciated.

References

(1) (a) Barybin M. V.; Meyers, J. J., Jr.; Neal, B. M. "Renaissance of Isocyanoarenes as Ligands in Low-Valent Organometallics," in *Isocyanide Chemistry - Applications in Synthesis and Material Science* Nenajdenko, V., Ed. Wiley-VCH: Weinheim, **2012**, pp 493-529. (b) Siemeling, U.; Klapp, L. R. R.; Bruhn, C. *Z. Anorg. Allg. Chem.* **2010**, *636*, 539. (c) Wrackmeyer, B.; Maisel, H. E.; Milius, W.; Herberhold, M. *Z. Anorg. Allg. Chem.* **2008**,

634, 1434. (d) Boyarskiy, V. P.; Bokach, N. A.; Luzyanin, K. V.; Kukushkin, V. Y. *Chem. Rev.* **2015**, *115*, 2698. (e) Holovics, T. C.; Deplazes, S. F.; Toriyama, M.; Powell, D. R.; Lushington, G. H.; Barybin, M. V. *Organometallics* **2004**, *23*, 2927.

(2) (a) Vecchi, A.; Erickson, N. R.; Sabin, J. R.; Floris, B.; Conte, V.; Venanzi, M.; Galloni, P.; Nemykin, V. N. *Chem. Eur. J.* **2015**, *21*, 269. (b) Sun, B.; Ou, Z.; Meng, D.; Fang, Y.; Song, Y.; Zhu, W.; Solntsev, P. V.; Nemykin, V. N.; Kadish, K. M. *Inorg. Chem.* **2014**, *53*, 8600. (c) Dammer, S. J.; Solntsev, P. V.; Sabin, J. R.; Nemykin, V. N. *Inorg. Chem.* **2013**, *52*, 9496. (d) Rohde, G. T.; Sabin, J. R.; Barrett, C. D.; Nemykin, V. N. *New J. Chem.*, **2011**, *35*, 1440. (e) Nemykin, V. N.; Galloni, P.; Floris, B.; Barrett, C. D.; Hadt, R. G.; Subbotin, R. I.; Marrani, A. G.; Zanoni, R.; Loim, N. M. *Dalton Trans.* **2008**, 4233. (f) Nemykin, V. N.; Barrett, C. D.; Hadt, R. G.; Subbotin, R. I.; Maximov, A. Y.; Polshin, E. V.; Koposov, A. Y. *Dalton Trans.* **2007**, 3378. (g) Loim, N. M.; Abramova, N. V.; Sokolov, V. I. *Mendeleev Commun.* **1996**, 46; (h) Burrell, A. K.; Campbell, W. M.; Jameson G. B.; Officer, D. L.; Boyd, P. D. W.; Zhao, Z.; Cocks, P. A.; Gordon, K. C. *Chem. Commun.* **1999**, 637; (i) Narayanan, S.J.; Venkatraman, S.; Dey, S. R.; Sridevi, B.; Anand, V. R. G.; Chandrashekar, T. K. *Synlett* **2000**, 1834; (g) Rhee, S. W.; Na, Y. H.; Do, Y.; Kim, J. *Inorg. Chim. Acta* **2000**, *309*, 49; (k) Shoji, O.; Okada, S.; Satake, A.; Kobuke Y. *J. Am. Chem. Soc.* **2005**, *127*, 2201; (l) Shoji, O.; Tanaka, H.; Kawai, T.; Kobuke, Y. *J. Am. Chem. Soc.* **2005**, *127*, 8598; (m) Auger, A.; Swarts, J. C. *Organometallics* **2007**, *26*, 102.; (n) Kubo, M.; Mori, Y.; Otani, M.; Murakami, M.; Ishibashi, Y.; Yasuda, M.; Hosomizu, K.; Miyasaka, H.; Imahori, H.; Nakashima, S. *J. Phys. Chem. A* **2007**, *111*, 5136. (o) Shoji, O.; Okada, S.; Satake, A.; Kobuke, Y. *J. Am. Chem. Soc.* **2005**, *127*, 2201. (p) Rochford, J.; Rooney, A. D.; Pryce, M. T. *Inorg. Chem.* **2007**, *46*, 7247. (q) Nemykin, V. N.; Rohde, G. T.; Barrett, C. D.; Hadt, R.

G.; Bizzarri, C.; Galloni, P.; Floris, B.; Nowik, I.; Herber, R. H.; Marrani, A. G.; Zanoni, R.; Loim, N. M. *J. Am. Chem. Soc.* **2009**, *131*, 14969. (r) Nemykin, V. N.; Rohde, G. T.; Barrett, C. D.; Hadt, R. G.; Sabin, J. R.; Reina, G.; Galloni, P.; Floris, B. *Inorg. Chem.* **2010**, *49*, 7497. (s) Galloni, P.; Floris, B.; de Cola, L.; Cecchetto, E.; Williams, R. M. *J. Phys. Chem. C* **2007**, *111*, 1517. (t) Solntsev, P. V.; Neisen, B. D.; Sabin, J. R.; Gerasimchuk, N. N.; Nemykin, V. N. *J. Porphyrins Phthalocyanines*, **2011**, *15*, 612; (u) Vecchi, A.; Gatto, E.; Floris, B.; Conte, V.; Venanzi, M.; Nemykin, V. N.; Galloni, P. *Chem. Commun.* **2012**, *48*, 5145.

(3) (a) Jin, Z.; Nolan, K.; McArthur, C. R.; Lever, A. B. P.; Leznoff, C. C. *J. Organomet. Chem.* **1994**, *468*, 205. (b) Poon, K.-W.; Yan, Y.; Li, X. Y.; Ng, D. K. P. *Organometallics* **1999**, *18*, 3528. (c) An, M.; Kim, S.; Hong, J.-D. *Bull. Korean Chem. Soc.* **2010**, *31*, 3272; (d) Gonzalez-Cabello, A.; Claessens, C. G.; Martin-Fuch, G.; Ledoux-Rack, I.; Vazquez, P.; Zyss, J.; Agullo-Lopez, F.; Torres, T. *Synthetic Metals* **2003**, *137*, 1487; (e) Gonzalez-Cabello, A.; Vazquez, P.; Torres, T. *J. Organomet. Chem.* **2001**, *637-639*, 751.

(4) (a) Vecchi, A.; Galloni, P.; Floris, B.; Dudkin, S. V.; Nemykin, V. N. *Coord. Chem. Rev.* **2015**, *291*, 95-171. (b) Vecchi, A.; Galloni, P.; Floris, B.; Nemykin, V. N. *J. Porphyrins Phthalocyanines* **2013**, *17*, 165. (c) Devillers, H.; Moutet, J.-C.; Royal, G.; Saint-Aman, E. *Coord. Chem. Rev.* **2009**, *253*, 21. (d) Suijkerbuijk, B. M. J. M.; Gebbink, R. J. M. K. *Angew. Chem. Int. Ed.* **2008**, *47*, 7396.

(5) Barybin, M. V.; Holovics, T. C.; Deplazes, S. F.; Lushington, G. H.; Powell, D. R.; Toriyama, M. *J. Am. Chem. Soc.* **2002**, *124*, 13668.

(6) (a) Muraoka, T.; Kinbara, K.; Aida, T. *Nature* **2006**, *440*, 512. (b) Bucher, C.; Bayley, C. H. *Nature* **2010**, *467*, 164. (c) Jurow, M.; Schuckman, A. E.; Batteas, J. D.; Drain, C. M. *Coord. Chem. Rev.*, **2010**, *254*, 2297.

(7) Nemykin, V. N.; Dudkin, S. V.; Fathi Rasekh, M.; Spaeth, A. D.; Rhoda, H. M.; Belosludov, R. V.; Barybin, M. V. *Inorg. Chem.* **2015**, 54, 10711-10724.

(8) Robinson, R. E.; Holovics, T. C.; Deplazes, S. F.; Powell, D. R.; Lushington, G. H.; Thompson, W. H.; Barybin, M. V. *Organometallics.* **2005**, 24, 2386-2397.

(9) (a) Hanack, M.; Kamenzin, S.; Kamenzin, C.; Subramanian, L. R. *Synth. Metals* **2000**, *110*, 93. (b) Hanack, M.; Hees, M.; Witke, E. *New J. Chem.* **1998**, *22*, 169. (c) Watkins, J. J.; Balch, A. L. *Inorg. Chem.* **1975**, *14*, 2720. (c) Vagin, S.; Ziener, U.; Hanack, M.; Stuzhin, P.A. *Eur. J. Inorg. Chem.* **2004**, 2877. (d) Pohmer, J.; Hanack, M.; Barcina, J.O. *J. Mater. Chem.* **1996**, *6*, 957. (e) Hanack, M.; Kang, Y. G. *Chem. Ber.* **1991**, *124*, 1607. (f) Galardon, E.; Lukas, M.; Le Maux, P.; Toupet, L.; Roisnel, T.; Simonneaux, G. *Acta Cryst. C* **2000**, *56*, 955 (g) Lee, F. W.; Choi, M. Y.; Cheung, K. K.; Che, C. M. *J. Orgnomet. Chem.* **2000**, *595*, 114. (h) Galardon, E.; Lukas, M.; Le Maux, P.; Simonneaux, G. *Tetr. Lett.* **1999**, *40*, 2753. (i) Geze, C.; Legrand, N.; Bondon, A.; Simonneaux, G. *Inorg. Chim. Acta.* **1992**, *195*, 73. (j) Mezger, M.; Hanack, M.; Hirsch, A.; Kleinwachter, J.; Mangold, K. M.; Subramanian, L. R. *Chem. Ber.* **1991**, *124*, 841.

(10) Galardon, E.; Le Maux, P.; Paul, C.; Poriel, C.; Simonneaux, G. *J. Organomet. Chem.* **2001**, *629*, 145.

(11) (a) Barriere, F.; Geiger, W. E. *J. Am. Chem. Soc.* **2006**, *128*, 3980; (b) Geiger, W. E.; Connelly, N. G. *Advances in Organometallic Chemistry* **1985**, *24*, 87.

(12) Barybin, M. V. *Coord. Chem. Rev.* **2010**, *254*, 1240.

(13) Gaussian 09, Revision **D.1**, Frisch, M. J.; Trucks, G. W.; Schlegel, H. B.; Scuseria, G. E.; *et al* Gaussian, Inc., Wallingford CT, **2009**. *For full citation, see Supporting Information*.

(14) Tenderholt, A. L. *QMForge, Version 2.1.* Stanford University, Stanford, CA, USA.

(15) (22) Tao, J. M.; Perdew, J. P.; Staroverov, V. N.; Scuseria, G. E. *Phys. Rev. Lett.* **2003**, *91*, 146401.

(16) (23) (a) Dunning Jr., T. H.; Hay, P. J. in: *Modern Theoretical Chemistry*, Ed. H. F. Schaefer III, Vol. 3, Plenum, New York, **1976**, pp. 1-28. (b) Fuentealba, P.; Preuss, H.; Stoll, H.; v. Szentpaly, L. *Chem. Phys. Lett.* **1982**, *89*, 418. (c) Fuentealba, P.; Stoll, H.; v. Szentpaly, L. ; Schwerdtfeger, P.; Preuss, H. *J. Phys. B* **1983**, *16*, L323-L28. (d) Stoll, H.; Fuentealba, P.; Schwerdtfeger, P.; Flad, J.; v. Szentpaly, L.; Preuss, H. *J. Chem. Phys.* **1984**, *81*, 2732.

(17) (a) Choy, C. K.; Mooney, J. R.; Kenney, M. E. *J. Magn. Res.* **1979**, *35*, 1. (b) Nemykin, V. N.; Kobayashi, N.; Chernii, V. Y.; Belsky, V. K. *Eur. J. Inorg. Chem.* **2001**, 733. (c) Ona-Burgos, P.; Casimiro, M.; Fernandez, I.; Navarro, A. V.; Fernandez Sanchez, J. F.; Carretero, A. S.; Gutierrez, A. F. *Dalton Trans.* **2010**, *39*, 6231. (d) Nemykin, V. N.; Chernii, V. Ya.; Volkov, S. V.; Bundina, N. I.; Kaliya, O. L.; Li, V. D.; Lukyanets, E. A. *J. Porphyrins Phthalocyanines* **1999**, *3*, 87. (e) Hanack, M.; Ryu, H. *Synth. Metals* **1992**, *46*, 113. (f) Nemykin, V. N.; Polshina, A. E.; Chernii, V. Y.; Polshin, E. V.; Kobayashi, N. *Dalton* **2000**, 1019.

(18) Nemykin, V. N.; Purchel, A. A.; Spaeth, A. D.; Barybin, M. V. *Inorg. Chem.*, **2013**, *52*, 11004.

(19) (a) Waluk, J.; Michl, J. *J. Org. Chem.* **1991,** *56*, 2729-2735. (b) Michl, J. *J. Am. Chem. Soc.* **1978,** *100*, 6801-6811. (c) Michl, J. *J. Am. Chem. Soc.* **1978,** *100*, 6812-6818. (d)

Ziegler, C. J.; Erickson, N. R.; Dahlby, M. R.; Nemykin, V. N. *J. Phys. Chem. A*, **2013**, *117*, 11499. (e) Ziegler, C. J.; Sabin, J. R.; Geier, G. R.; Nemykin, V. N. *Chem. Commun.*, **2012**, *48*, 4743. (f) Sripothongnak, S.; Ziegler, C. J.; Dahlby, M. R.; Nemykin, V. N. *Inorg. Chem.*, **2011**, *50*, 6902.

(20) (a) Kobayashi, N.; Muranaka, A.; Mack, J. *Circular Dichroism and Magnetic Circular Dichroism Spectroscopy for Organic Chemists*, RSC London, UK, **2012**, 216. (b) Mason, W. R. *A Practical Guide to Magnetic Circular Dichroism Spectroscopy*, John Wiley & Sons, Inc., Hoboken, N. J.; **2007**, 223. (c) Kobayashi, N.; Fukuda, T. *Bull. Chem. Soc. Japan.* **2009**, *82*, 631.

(21) (a) Speak, A.; Appl, J. *Cryst.* **2003**, 36, 7-13. (b) van der Sluis P. & Spek A. L. *Acta Cryst.* **1990**, A46, 194-201

(22) (a) Barybin M. V.; Meyers, J. J., Jr.; Neal, B. M. "Renaissance of Isocyanoarenes as Ligands in Low-Valent Organometallics," in *Isocyanide Chemistry - Applications in Synthesis and Material Science* Nenajdenko, V., Ed. Wiley-VCH: Weinheim, **2012**, pp 493-529. (b) Siemeling, U.; Klapp, L. R. R.; Bruhn, C. *Z. Anorg. Allg. Chem.* **2010**, *636*, 539. (c) Wrackmeyer, B.; Maisel, H. E.; Milius, W.; Herberhold, M. *Z. Anorg. Allg. Chem.* **2008**, *634*, 1434. (d) Boyarskiy, V. P.; Bokach, N. A.; Luzyanin, K. V.; Kukushkin, V. Y. *Chem. Rev.* **2015**, *115*, 2698. (e) Holovics, T. C.; Deplazes, S. F.; Toriyama, M.; Powell, D. R.; Lushington, G. H.; Barybin, M. V. *Organometallics* **2004**, *23*, 2927.

(23) (a) Gouterman, M. *J. Mol. Spectrosc.* **1961,** *6*, 138-163. (b) Gouterman, M.; Wagnière, G.H.; Snyder, L.C. *J. Mol. Spectrosc.* **1963,** *11*, 108-127.